Electromagnetic surface modes of a dielectric superlattice: the supercell method

F. Ramos-Mendieta

Centro de Investigación en Física de la Universidad de Sonora, Apartado Postal 5-088, Hermosillo, Sonora 83190, México

P. Halevi

Instituto de Física de la Universidad Autónoma de Puebla, Apartado Postal J-48, Puebla, Puebla 72570, México, and Instituto Nacional de Astrofísica, Optica y Electrónica, Apartado Postal 51, Puebla, Puebla 72000, México

Received March 8, 1996

We present a study of the reliability of the supercell method in calculations of surface electromagnetic modes. For a truncated superlattice constituted of nonabsorbing dielectric layers, we demonstrate that the numerical solutions obtained by this method for transverse-electric waves agree with those based on the Bloch theory for the semi-infinite superlattice. A slab of superlattice with at least nine unit cells yields satisfactory convergence to an analytic dispersion relation for the surface modes. In addition, we apply the supercell method to study in detail the dependence of transverse-electric and transverse-magnetic surface waves on the cut-off position in the cell next to the surface. As a specific case, we choose a TiO_2/SiO_2 superlattice—layers with relatively high dielectric contrast in the visible spectrum. We find the surface modes strongly dependent on the position of the surface. In fact, they appear only for certain terminations. By plotting the field amplitudes, we show that there exist different possibilities for the guidance of surface waves. The variation of the penetration depth of these modes is also discussed. © 1997 Optical Society of America [S0740-3224(97)01302-7]

1. INTRODUCTION

In the past two decades a large amount of theoretical and experimental work has been carried out to study semiconductor and metallic superlattices. In these artificial media, composed of alternating layers of different materials with thicknesses of approximately 1–500 nm, the collective excitations that define their physical properties (phonons, plasmons, and polaritons) are now very well studied phenomena.[1–3] Their fabrication has been performed by use of modern crystal-growth techniques (such as molecular-beam epitaxy), and, because of their unusual properties, superlattices are widely applied in the design of optical and optoelectronic devices such as bandpass filters, mirrors, and quantum-well lasers. Available growth technologies can synthesize multilayered structures with very well controlled heterointerfaces and layers.[4,5]

In a superlattice the propagation of electromagnetic waves is described by band theory. With nonabsorbing layers, the bands are caused by the coherent interference of the reflected waves in every superlattice layer. If the constitutive materials are dispersive (frequency dependence of refractive indices), the polariton energy bands are the result of the interplay between the wave diffraction in the periodic structure and their coupling with the elementary excitations in the layers. In both cases, theoretical calculations are based on the Bloch theory, and the methods of Fourier series, transfer matrix, or Green functions are used.[6–10]

If the symmetry of the superlattice is reduced by the introduction of lattice imperfections or (external) surfaces, new methods of calculations must be developed. In particular, the presence of a surface modifies the superlattice band structure by introducing new electromagnetic states. These new solutions, the surface modes, are characterized by decaying fields in both perpendicular directions away from the interface between the semi-infinite superlattice and the air. The understanding of the surface properties in a superlattice is of particular importance because, by choosing a proper termination of the structure, it is possible, for example, to eliminate the losses associated with radiation into surface modes.[11]

Surface waves in dielectric superlattices were predicted almost three decades ago.[12] Subsequently, experiments with $GaAs/Al_{0.2}Ga_{0.8}As$ superlattices[13,14] and ZnS/cryolite superlattices[15] proved their existence. On the theoretical side, an analytic expression for the dispersion relation $\omega(\beta)$ was obtained by use of the Bloch theorem with a complex Bloch wave vector κ in the semi-infinite superlattice and by matching this solution with an exponentially decaying wave in the air.[6] Most of the theoretical studies for acoustic surface modes,[1] surface plasmon polaritons,[16] and surface electronic states[17] in superlattices were based on the application of similar ideas. However, only a few years ago,[18] complete dispersion curves for surface electromagnetic modes in dielectric superlattices were published.

In this paper we calculate dispersion relations of transverse-electric (TE) and transverse-magnetic (TM) surface waves, realized with the supercell method. As

0740-3224/97/020370-12$10.00

we shall see, our results are not in agreement with those in Ref. 18, but the agreement with the solutions generated by the formalism of Ref. 19 is very good. Further, we shall give numerical proof of the convergence of our results (essentially the surface modes of a superlattice slab) to those of a semi-infinite superlattice in which the method of calculation requires complex Bloch wave vectors.[19] This coincidence gives credence to the supercell method in surface electromagnetic mode calculations.

The dispersion relation of a surface mode depends on lattice parameters, on the dielectric constants of the media and, most sensitively, on the cut-off position in the surface cell. Other than a brief report,[20] we have not found previous calculations based on the Bloch formulation considering an arbitrary cut (parallel to the layers) to define the surface, as in this work. However, there exists another formulation for an arbitrary slab superstrate on a semi-infinite superlattice that could, in principle, lead to similar solutions.[1] The corresponding problem for lattice vibrations was explored in Ref. 21. The surface cell (possibly not a complete unitary cell) is the main guide of the surface mode and is bounded on one side by air and on the other by the semi-infinite superlattice.

The supercell method that we use for calculations is based on the Fourier theory. This is a numerical method to deal with aperiodic configurations within the framework of the Bloch theorem. Rather than studying surface modes in a semi-infinite superlattice, we calculate the surface modes in a superlattice slab. The method has been recently used in calculations of surface modes in more complicated dielectric structures with two-dimensional and three-dimensional periodicities where analytic methods do not exist.[11,22] However, the relation between surface modes in a semi-infinite photonic crystal and surface modes in a crystal slab has not been investigated. Thus the accuracy of the supercell method is an open question. One aim of the present work is to establish the supercell method as an alternative to the semi-analytical method based on the Bloch theorem. Another purpose is to present a detailed study of the dependence of the surface modes on the cut-off position of the surface cell, as well as on other parameters.

In all our calculations we use a supercell that contains a slab of superlattice centered between two air regions. If this supercell is repeated throughout space, one generates a periodic superstructure constituted by slabs of superlattice alternating with air slabs. For an accurate computation of the surface modes two considerations must be taken into account in the construction of the supercell. First, the bound states associated with each superlattice slab do not overlap with the states of the neighboring slabs provided that the air regions are wide enough, and second, the surface modes on both sides of a slab do not interact if the slab is constituted by a large enough number of unitary cells. With these considerations the Bloch theorem applied to solve the Maxwell equations in this superstructure gives rise to an energy-band structure. Some of these bands are associated with the surface modes and, in the limit of a large supercell, the frequencies $\omega(\beta)$, where β is the propagation vector, are expected to converge to those of the surface modes of a semi-infinite superlattice. In this limit the solution for a surface mode that we find can be considered infinitely degenerate.

The rest of the paper is organized as follows. In Section 2 we use the plane-wave expansion method in order to solve the Maxwell equations for both TE and TM polarizations. General expressions to compute the dispersion relations of the bulk and the surface waves are obtained. In Section 3 the numerical results are presented. We validate the use of the supercell method by comparing the surface-mode solutions derived by this method with those obtained for a semi-infinite superlattice. Additionally, we compute the surface electromagnetic modes for a TiO_2/SiO_2 superlattice, investigating their behavior when the termination of the superlattice is varied. In Section 4 the conclusions of the work are given.

2. THEORY

The starting point for our calculations are Maxwell's equations:

$$\nabla \times \mathbf{E} = i\,\frac{\omega}{c}\,\mathbf{B}, \quad \nabla \times \mathbf{H} = -i\,\frac{\omega}{c}\,\epsilon(x)\mathbf{E}, \tag{1}$$

where the oscillations of the fields have the form $\exp(-i\omega t)$ and the dielectric constant ϵ is position dependent. For both bulk and surface calculations there is translational invariance along the axes y and z and periodicity along the x direction. Periodicity in the surface problem arises from the infinite repetition of the fictitious supercell used in the method (see Subsection 2.B). For this geometry there are two independent vibration modes when the propagation is in the x–y plane. One is the TE mode with the electric field polarized parallel to the z axis. The other is the TM mode with the electric field parallel to the x–y plane. From Eqs. (1) we find the wave equations for the transverse fields $E(x, y)$ (TE) and $H(x, y)$ (TM):

$$\frac{1}{\epsilon(x)}\left(\frac{\partial^2}{\partial x^2} + \frac{\partial^2}{\partial y^2}\right)E = -\frac{\omega^2}{c^2}\,E, \tag{2}$$

$$\left[\frac{\partial}{\partial x}\,\frac{1}{\epsilon(x)}\,\frac{\partial}{\partial x} + \frac{1}{\epsilon(x)}\,\frac{\partial^2}{\partial y^2}\right]H = -\frac{\omega^2}{c^2}\,H. \tag{3}$$

To solve Eqs. (2) and (3), we apply the Bloch theorem, which states that in a periodic medium the fields can be written as the product of two functions. The first is a wavelike part, and the second is a cell-periodic part. By using an orthogonal plane-wave basis, we can write

$$A_\kappa(x, y) = \sum_G A_\kappa(G)\exp[i(\kappa + G)x]\exp(i\beta y), \tag{4}$$

where κ is the one-dimensional Bloch wave vector. In Eq. (4), $A_\kappa(x, y)$ is the amplitude $E(H)$ of the electric (magnetic) field for TE (TM) polarization, the summation extends over the infinite reciprocal lattice vectors of amplitude G, and β is the propagation constant along the y direction.

The dielectric function (and its inverse) are periodic. We use the same orthogonal plane basis to expand it in Fourier series. Hence

$$\frac{1}{\epsilon(x)} = \sum_G \mu_G \exp(iGx). \tag{5}$$

If Eqs. (4) and (5) are substituted in Eqs. (2) and (3), after some algebraic manipulations and considering that the functions $\exp(-iGx)$ and $\exp(-iG'x)$ are orthonormal in the unit cell, one obtains

$$\sum_{G'} \mu_{G-G'}[(\kappa + G')^2 + \beta^2]E_\kappa(G') = \frac{\omega^2}{c^2} E_\kappa(G) \quad (TE), \tag{6}$$

$$\sum_{G'} \mu_{G-G'}[(\kappa + G)(\kappa + G') + \beta^2]H_\kappa(G') = \frac{\omega^2}{c^2} H_\kappa(G) \quad (TM). \tag{7}$$

If we allow G to take all the points of the reciprocal lattice, then Eqs. (6) and (7) are each an infinite set of linear equations for the eigenvectors E_κ and H_κ. For given values of the Bloch wave vector κ and the propagation constant β, each set of equations has solutions for some eigenvalues $\omega_j(\kappa, \beta)$, where the band index $j(= 1,2,\ldots)$ specifies the different oscillation modes of the electromagnetic fields. On the other hand, by fixing the value of β and running κ through the first Brillouin zone, one can obtain the band structure and determine the ranges of frequency where oscillations with real κ do *not* exist. These regions with complex κ are the forbidden gaps. They are the frequency regions at which the surface modes can be located. With the positive semiaxis x pointing inward, the fields in the semi-infinite superlattice require a positive imaginary part for the Bloch wave vector κ to ensure the correct decay behavior. For a given frequency the real part of κ is restricted to the first Brillouin zone.

The sets of equations represented in Eqs. (6) and (7) can be seen as two eigenvalue problems of the form $\mathbf{Mx} = \lambda^2\mathbf{x}$. The eigenvalues and eigenvectors are obtained by a process of numerical diagonalization. For the cell in the bulk problem and the supercell in the surface problem we will consider a dielectric function with central symmetry. Thus by inspection of Eqs. (6) and (7) we find that the matrices involved are Hermitian only for the TM case. Nevertheless, for both polarizations the eigenvalues are real quantities.

In order to realize a more complete study of the properties of surface modes, it is useful to rewrite Eqs. (6) and (7) with the propagation constant β as the eigenvalue. Thus we can calculate $\beta(\omega)$ rather than $\omega(\beta)$. To transform the equations to this form, a matrix inversion will be required.

A. Bulk Modes

We calculate the electromagnetic modes of the infinite superlattice with the unitary cell shown in Fig. 1(a). The system is an infinite array of alternating layers with dielectric functions ϵ_a and $\epsilon_b(\epsilon_a > \epsilon_b)$ with layer thicknesses a and b, respectively. Thus the guiding layers of dielectric constant ϵ_a are separated by a distance b. The cell is defined in the interval $-d/2 < x < d/2$, where $d = a + b$ is the period. The dielectric function can be written as

$$\epsilon(x) = \epsilon_b + (\epsilon_a - \epsilon_b)\Theta\left(\frac{a}{2} - |x|\right), \tag{8}$$

where $\Theta(\alpha)$ is the Heaviside function ($\Theta = 1$ for $\alpha \geq 0$, $\Theta = 0$ for $\alpha < 0$). Of course, the spatial dependence in Eq. (8) is also valid for the inverse of the dielectric function. Thus the Fourier coefficients are

$$\mu_G = \frac{1}{d}\int_{-d/2}^{d/2} \frac{1}{\epsilon(x)} \exp(-iGx)dx = \frac{1}{\epsilon_b}\delta_{G,0} + \left(\frac{1}{\epsilon_a} - \frac{1}{\epsilon_b}\right) f \frac{\sin(Ga/2)}{Ga/2}, \tag{9}$$

where $f = a/d$ is the filling fraction of the denser dielectric a and δ is the Kronecker delta function. Equation (9) must be substituted in Eqs. (6) and (7) with the reciprocal lattice vectors $G = 2\pi m/d$, where $m = \ldots,-2,-1,0,1,2,\ldots$, to obtain the numerical solution.

B. Supercell Representation for Surface Modes

Now we consider the effect of truncation of the superlattice. The real system is constituted by a semi-infinite superlattice ($0 \leq x < \infty$) and air or some bounding medium ($-\infty < x < 0$), as is shown in Fig. 1(b). For this configuration the Bloch theorem cannot be applied because the surface has broken the periodicity. However, by the construction of a fictitious, infinite superstructure with slabs of superlattice alternated with slabs of air, it is possible to

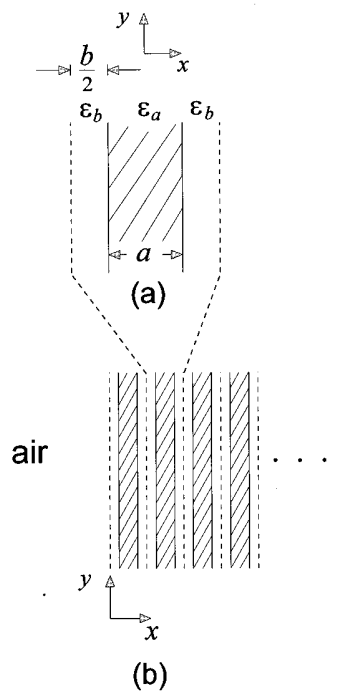

Fig. 1. (a) Geometry of the unit cell of width $d = a + b$. The repetition of this cell along the x axis generates an infinite superlattice constituted of alternating layers of dielectric constants ϵ_a and ϵ_b with thicknesses a and b, respectively. (b) Geometry of the semi-infinite superlattice bounded by air.

use the Bloch theory to calculate the modes confined in each slab of superlattice. Two of these modes have surface character, and if the conditions discussed at the end of Section 1 are satisfied, we can expect that the results of the calculation approximate reasonably well the surface modes of the real truncated superlattice.

We use a supercell constituted by a superlattice slab of thickness $l = (n + 2\tau)d$ limited on both sides by air slabs of width l_0 (see Fig. 2). Here n represents the number of complete inner cells and τd is the width of the surface cell; τ $(0 \leqslant \tau \leqslant 1)$ is the cut parameter. The slab is symmetric with respect to its center. Thus our supercell has a width $L = l + 2l_0$. The inverse dielectric constant may be written, in analogy to Eq. (8), as

$$\frac{1}{\epsilon(x)} = \frac{1}{\epsilon_0} + \left[\frac{1}{\epsilon'(x)} - \frac{1}{\epsilon_0}\right]\Theta\left(\frac{l}{2} - |x|\right), \tag{10}$$

where ϵ_0 is the dielectric constant of air (or of the bounding medium) and $1/\epsilon'$ is given by

$$\frac{1}{\epsilon'(x)} = \frac{1}{\epsilon_b} + \left(\frac{1}{\epsilon_a} - \frac{1}{\epsilon_b}\right)\left[F(x) + \sum_{x_j} \Theta\left(\frac{a}{2} - |x - x_j|\right)\right]. \tag{11}$$

In this equation, x_j are the center positions of the *inner* cells of the superlattice slab. The function $F(x)$ depends on the cutoff position of the surface cells. Considering the three topologically different truncations (see Fig. 3), we can write

$$F(x) = \begin{cases} 0 & 0 < \tau d \leqslant b/2 \quad (a) \\ \displaystyle\sum_{x_j'} \Theta\left(\frac{\tau d - b/2}{2} - \left|x - x_j'\right|\right) & b/2 < \tau d \leqslant b/2 + a \quad (b) \\ \displaystyle\sum_{x_j'} \Theta(a/2 - |x - x_j'|) & b/2 + a < \tau d \leqslant d \quad (c) \end{cases}, \tag{12}$$

where x_j' are the center positions of the truncated or complete layers with dielectric constant ϵ_a in the two surface cells. In Fig. 3 we can see that in cases (a) and (c) a layer with dielectric constant ϵ_b is the surface layer. On the other hand, in case (b) the surface layer is one with dielectric constant ϵ_a.

The Fourier coefficients for the superlattice of supercells are calculated from the equation

$$\mu_G = \frac{1}{L}\int_{-L/2}^{L/2} \frac{1}{\epsilon(x)} \exp(-iGx)dx. \tag{13}$$

With the substitution of Eq. (10) we obtain the result

$$\mu_G = \left[\frac{1}{\epsilon_0} + \left(\frac{1}{\epsilon_b} - \frac{1}{\epsilon_0}\right)\frac{l}{L} + \left(\frac{1}{\epsilon_a} - \frac{1}{\epsilon_b}\right)\left(\frac{na}{L} + \mathscr{F}_1\right)\right]\delta_{G,0} + \left[\left(\frac{1}{\epsilon_b} - \frac{1}{\epsilon_0}\right)\frac{l}{L}\frac{\sin(Gl/2)}{Gl/2}\right](1 - \delta_{G,0}) + \left\{\left(\frac{1}{\epsilon_a} - \frac{1}{\epsilon_b}\right)\left[\frac{a}{L}\frac{\sin(Ga/2)}{Ga/2}\sum_{x_j} \exp(-iGx_j) + \mathscr{F}_2\right]\right\} \times (1 - \delta_{G,0}), \tag{14}$$

where the functions $\mathscr{F}_1$ and $\mathscr{F}_2$ are

$$\mathscr{F}_1(x) = \begin{cases} 0 & 0 \leqslant \tau d < b/2 \\ \dfrac{2(\tau d - b/2)}{L} & b/2 \leqslant \tau d < b/2 + a \\ \dfrac{2a}{L} & b/2 + a \leqslant \tau d < d \end{cases}, \tag{15}$$

$$\mathscr{F}_2(x) = \begin{cases} 0 & 0 \leqslant \tau d < b/2 \\ \dfrac{2(\tau d - b/2)}{L}\dfrac{\sin[G(\tau d - b/2)/2]}{G(\tau d - b/2)/2}\cos(Gx_j') & b/2 \leqslant \tau d < b/2 + a \\ \dfrac{2a}{L}\dfrac{\sin(Ga/2)}{Ga/2}\cos(Gx_j') & b/2 + a \leqslant \tau d < d \end{cases}. \tag{16}$$

The surface problem is thus reduced to the solution of Eqs. (6) and (7) with the coefficient μ_G expressed in Eq. (14). It must be noted that reciprocal lattice vectors now have the form $G = 2\pi m/L$.

3. NUMERICAL RESULTS

A. Supercell Method Reliability

Regarding the dispersion relations of surface modes, we mentioned previously the conditions to be satisfied in the construction of the appropriate supercell. Thus, if $l(n)$ and l_0 are sufficiently large (see Fig. 2), we should be able to reproduce the solutions calculated by other methods for truncated superlattices. We found dispersion curves $\omega(\beta)$ for surface modes only in Ref. 18. In this reference the fields penetrating into the semi-infinite superlattice

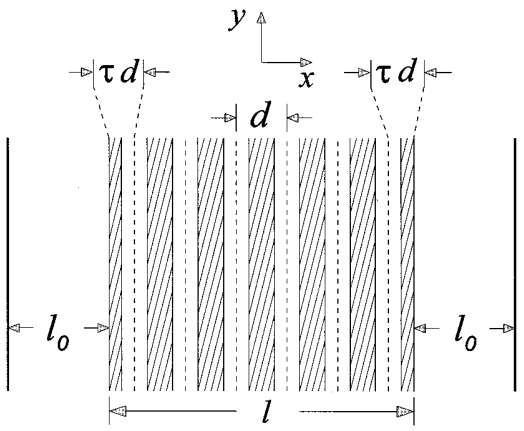

Fig. 2. Geometry of a supercell of width L. This symmetric structure contains one slab of superlattice (width l) bounded by two air layers of thickness l_0 each. The inner cells (here $n = 5$) and the two surface cells (incomplete unit cells) give the slab width $l = (n + 2\tau)d$. Thus $L = l + 2l_0$.

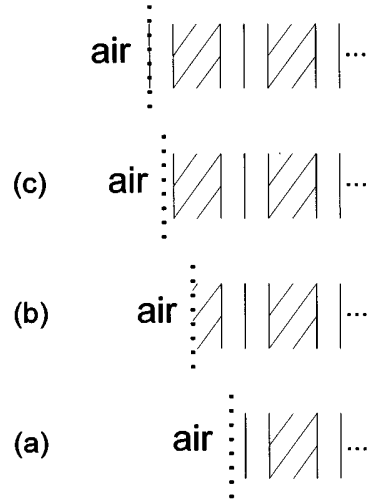

Fig. 3. Schematic representation for the termination of the superlattice. The dotted line is the position of the surface. Each figure shows both the surface cell of thickness τd and the first inner cell. In the uppermost figure, $\tau = 1$, the surface cell is a complete unit cell. (a) $0 \leq \tau < b/2d$; the surface cuts the superlattice through the inner ϵ_b layer of the original complete surface cell. (b) $b/2d \leq \tau < b/2d + a/d$; the termination is realized through the ϵ_a layer. (c) $b/2d + a/d \leq \tau < 1$; the surface cuts the superlattice through the outermost layer of dielectric constant ϵ_b. In each of the last three figures the surface cell is a portion of the unitary cell.

are assumed to be modulated by an envelope function that decays exponentially away from the surface. By using the same (unrealistic) dielectric constants for the layers,[18] we made a systematic study employing the supercell method; however, we were not able to reproduce the curves of Figures 1 and 2 of Ref. 18. We used slabs of superlattice with up to 21 cells and an expansion of 751 plane waves [G' terms in Eqs. (6) and (7)] for the fields. On the other hand, it should be said that the solutions plotted in Fig. 1 of Ref. 18 do agree with those obtained with the formalism of Ref. 19 provided that, in the latter reference, we change the sign of the complex Bloch wave vector. This, however, corresponds to unphysical solutions with an exponentially increasing amplitude toward the interior of the superlattice.

In Ref. 19 there may be found an alternative formulation of the topic of surface modes of a superlattice. In this reference the dispersion relation is given by Eq. (11.5-6); however, it is not plotted there. We graphed the solutions of this equation and compared them with the dispersion relation obtained by means of the supercell method. We found very good agreement between the two solutions for a sufficiently large number of unit cells n in the supercell. The parameters used are the following: $\epsilon_a = 11.4244$, $\epsilon_b = 8.3521$, $\epsilon_0 = 1.0$, and $\tau d = b/2 + a$. The dielectric constants correspond to a relatively low dielectric contrast ($\epsilon_a/\epsilon_b = 1.36$) in the far infrared. τd is selected considering that in Ref. 19 the superlattice terminates with a complete layer of dielectric constant ϵ_a.

Now we compare the solutions obtained with both methods. Figures 4(a) and 4(b), corresponding to TE waves, show the variation of the $j = 1$ band when the thickness b is increased for a fixed a. In these two figures we use the reduced frequency $\omega a/c$, the reduced propagation constant βa, and the reduced Bloch wave

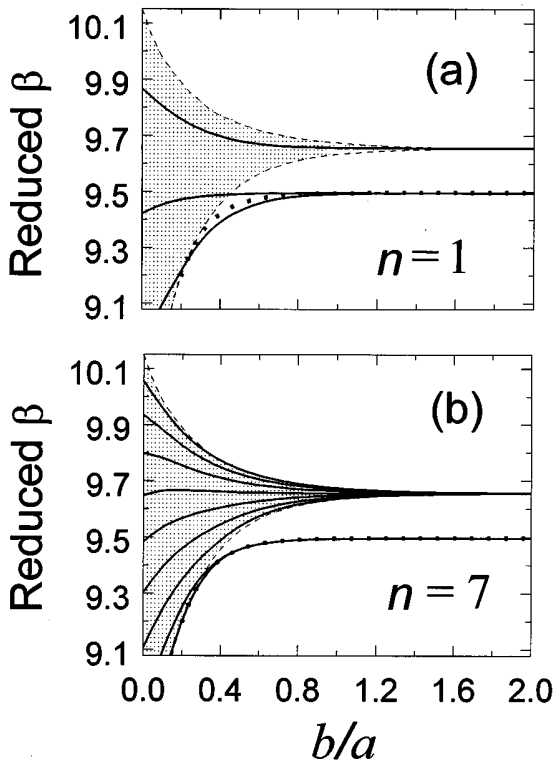

Fig. 4. TE surface modes calculated by the supercell method (continuous curves) and by Eq. (11.5-6) of Ref. 17 (dotted curve). See text for material parameters. The shaded zone represents the first bulk band for $\beta > \omega\epsilon_b^{1/2}/c$ at $\omega a/c = \pi$. Dashed curves are the band edges. The cut parameter is $\tau d = b/2 + a$. (a) Solutions obtained with one inner cell. Only for large separations ($b > a$) do the surface modes in the slab converge to that of the semi-infinite superlattice. (b) Solutions with seven inner cells. The equivalence of both methods is much better. Only for small separations ($b/a \leq 0.35$) do the two surface modes in the slab have appreciable interaction.

vector κa. Here $a = \lambda/2$, the separation b is normalized with a, and $\omega a/c = \pi$. Note that the last condition implies that we are solving an eigenvalue problem for β_j, as commented on in Section 2. In both figures the shaded zones delimited by dashed curves (the band edges) are the bulk bands, the dotted curves are the surface-mode dispersion relations obtained with Eq. (11.5-6) of Ref. 19, and the continuous lines represent the supercell solutions calculated with an expansion of 451 plane waves. In both figures we observe that the bulk-band width is diminished as b/a is increased, as expected. In fact, in the limit of very large separation b between the guiding layers ϵ_a, the band-edge envelopes converge to the eigenvalue of an isolated slab of dielectric constant ϵ_a with the two bounding media of dielectric constant ϵ_b. We note that the supercell method leads to a set of discrete solutions. The number of modes is the same as that of the total number of cells (the inner cells plus the two surface cells) contained in the supercell, that is, 3 and 9 for Figs. 4(a) and 4(b), respectively.

In Fig. 4(a), with $n = 1$ (supercell with two surface cells and one complete inner cell), we find three guided modes propagating in the slab of superlattice. For very low values of separation between the larger dielectric constant layers ($b/a \lesssim 0.22$), the fields of all three modes have bulk character. With increasing b/a, two of these modes change their behavior, acquiring surface-mode character. Of course, $n = 1$ corresponds to a very thin superlattice slab, and the two surface modes, one at each surface of the slab, interact strongly for a large range of b/a values. Only for $b/a \gtrsim 1.1$ do we see that the surface solutions of both methods are essentially in agreement. For very large separation these solutions converge to that of a single layer of dielectric constant ϵ_a bounded by air on one side and a medium with dielectric constant ϵ_b on the other; clearly, then, the size of the superlattice slab plays no role.

Figure 4(b) shows the results when the number of inner cells in the superlattice slab is increased to $n = 7$. Clearly the agreement of the two methods is better. Now the interaction of the surface modes across the slab practically disappears for b/a larger than 0.4. Continuing the process of increasing n, we did not observe an appreciable difference between the two methods of calculation when the slab of superlattice reached 15 inner cells. On the scale of Fig. 5 the differences cannot be resolved, being less than 1%. This accuracy suggests that the supercell method is quite reliable, for arbitrary b, if n is large enough. As we discuss below, in the air the fields of the surface modes are very confined to the surface. Thus even rather small values of the air thickness l_0 give a good fit. In Figs. 4(a) and 4(b) we chose $l_0 = 0.5l$.

B. Electromagnetic Surface Modes in a TiO_2/SiO_2 Superlattice

Now we apply the supercell method to study the surface modes in a superlattice constituted of alternated TiO_2 and SiO_2 layers. The dielectric constants are $\epsilon_a = 5.5225$ and $\epsilon_b = 2.1316$, respectively. These materials correspond to a relatively high dielectric contrast ($\epsilon_a/\epsilon_b = 2.59$) in the visible spectrum and were recently used in the construction of a quasiperiodic superlattice to observe, by an interferometric process, the dispersion relation of photons propagating through a Fibonacci lattice.[5] The results that we shall discuss provide the general, qualitative behavior of the surface modes that we also found in calculations with other constitutive materials for the superlattice. In the rest of the paper we redefine the reduced frequency as $\omega d/2\pi c$, the reduced propagation constant as $\beta d/2\pi$, and the reduced Bloch wave vector as $\kappa d/2\pi$. The filling fraction f and the cut parameter τ are the parameters to select. We chose a filling fraction $f = 0.66$ ($b = 0.5a$) and $\tau = 0.75$ (i.e., the surface layer is an ϵ_a layer of thickness $0.875a$). The position of the surface corresponds to Fig. 3(b). The number of complete cells in the slab used in the construction of the supercell is $n = 9$. The results that follow were obtained with an expansion of 251 (651) plane waves for the bulk (surface) problem. In all numerical calculations we find very well converged solutions by using reasonable computer time.

The dispersion relation of the surface modes can lie only in specific regions of the plane β–ω. In the air the fields decay away from the surface only when the relation $\beta > \omega\epsilon_0^{1/2}/c$ is satisfied. This is the necessary condition to obtain an imaginary normal component of the air wave vector. In a simple waveguide (material ϵ_a bounded by air on one side and material ϵ_b on the other side) the condition $\beta > \omega\epsilon_b^{1/2}/c$, for exponential decay in the substrate, must be also satisfied. On the other hand, in the superlattice the condition for decay is that the Bloch wave vector be complex (corresponding to bulk band gaps), with a positive imaginary part. In Fig. 5(a) we plot the TE bulk-band solutions of the superlattice and two light

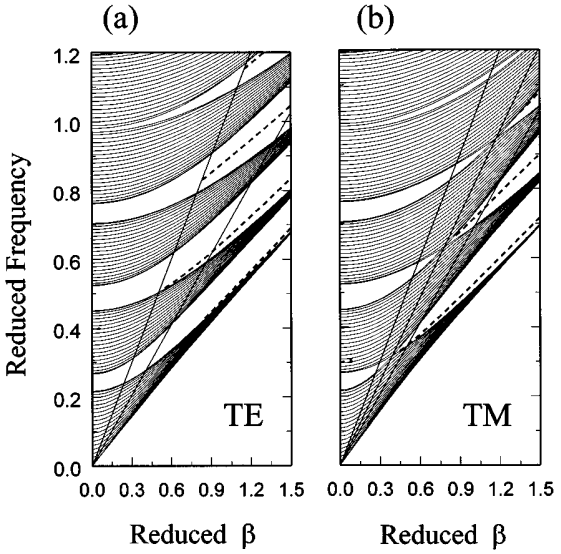

Fig. 5. Electromagnetic modes of a TiO_2/SiO_2 superlattice. The shaded zones are the bulk bands. Dashed curves are the surface modes. The larger-slope continuous line is the ϵ_0 light line ($\beta = \omega\epsilon_0^{1/2}/c$). The lower-slope continuous line is the ϵ_b light line ($\beta = \omega\epsilon_b^{1/2}/c$). With $b = 0.5a$ the cut parameter $\tau = 0.75$ represents a termination with a surface layer of dielectric constant ϵ_a of thickness $0.875a$ [see Fig. 3(b)]. The figures show the different locations of the dispersion curves of the surface modes in the four lowest band gaps: (a) TE modes and (b) TM modes. The line satisfying the Brewster condition is also plotted.

lines: the air light line and the ϵ_b light line. The first line (of the higher slope) delimits the oscillatory and the decaying behaviors of the fields in the air and is the graph of the equation $\beta = \omega\epsilon_0^{1/2}/c$. As we discuss below, the second line separates the character of the surface solutions. Thus the surface modes can appear only in the band gaps localized to the right side of the air light line and are different depending on their location to the right or to the left of the ϵ_b light line, $\beta = \omega\epsilon_b^{1/2}/c$. There is another line, the ϵ_a light line, not shown in Fig. 5(a), that delimits the region of physical solutions. This line coincides with the lower edge of the first (lowest) bulk band and has the slope $c/\epsilon_a^{1/2}$. All of these considerations are analogous for TM modes, shown in Fig. 5(b).

We note that in Fig. 5(b) the forbidden band gaps shrink to zero for some values of β. This phenomenon has to do with the Brewster condition and can be understood as follows. In a superlattice the band gaps result from the destructive interference among the waves scattered by all the layers. Consider an incident and a reflected wave in any one of the layers with dielectric constant ϵ_b. When $\beta(\equiv\beta_B) = (\omega/c)\epsilon_b^{1/2}\sin\theta_B$, where the Brewster angle is given by $\theta_B = \tan^{-1}(\epsilon_a/\epsilon_b)^{1/2}$, the coupling of these two waves in the low-dielectric-constant layers is frustrated because there are no reflected waves. Under these conditions, stationary waves and band gaps in the structure cannot be obtained because of the lack of interfering waves. This means that for any frequency ω, if $\beta \simeq \beta_B(\omega)$, the waves must be propagating in character. Thus, all the band gaps are closed. In Fig. 5(b) we also plot the line $\beta = \beta_B(\omega)$ representing the Brewster condition.

In addition, in Figs. 5(a) and 5(b) we present the dispersion relations of the surface modes appearing in every band gap. The qualitative behavior is different for each one. In the TE case the lowest surface mode almost coincides with the upper edge of the lowest bulk band, but in the upper band gap the modes appear very close to the lower edge of the fifth bulk band. For the other gaps the surface modes are more separated from the bulk solutions. In the TM case the surface modes can also start from the upper or from the lower bulk band bounding a band gap. Furthermore, the modes can begin at the points where the boundary curves of the bands cross. Although in this figure the surface modes do not appear to the left side of the crossing points, they may occur for other parameters.

The surface modes are more separated in frequency from the limits of the neighboring bulk bands when β is increased. This behavior occurs only for β values on the scale of Figs. 5(a) and 5(b). In fact, for very large β all the modes (bulk and surface modes) converge to the ϵ_a light line. This can be understood as follows. In the large β regime the bulk-band width decreases as a consequence of the lower overlapping between the fields guided by the neighboring ϵ_a layers. Hence in the limit $\beta d \to \infty$ the bulk bands are reduced to (infinitely degenerate) modes that correspond to light guided by a single ϵ_a slab of thickness a in a host medium of dielectric constant ϵ_b. The curves of dispersion for all these modes converge asymptotically to the ϵ_a light line (this is a result known for a homogeneous dielectrics slab). Then, because the surface modes are mainly guided by the ϵ_a layer of the surface cells (which have a different thickness from that of the ϵ_a layer of the bulk cells), their curves of dispersion must converge to the same ϵ_a light line. As we will see in Subsection 3.C, this behavior is not a general rule because the surface mode can also be guided by the ϵ_b layer.

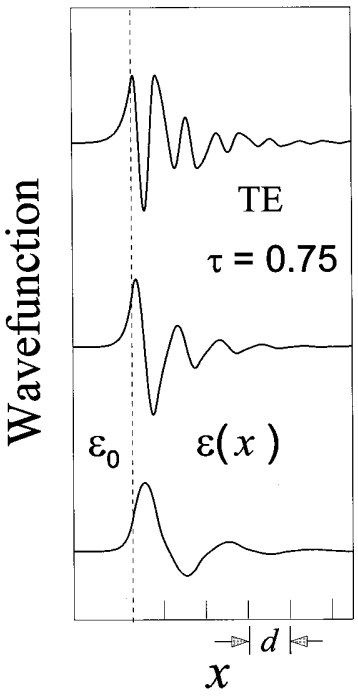

Fig. 6. Electric-field profiles Re(E) of the lower three TE surface modes of a TiO_2/SiO_2 superlattice. They correspond to the modes in the lower three band gaps of Fig. 5(a) at $\beta = 1.2$. At the bottom of the figure the separation between the arrows represents the width of the unit cell. The modes are mainly guided by the incomplete ϵ_a layer of thickness $0.875a$. Only the uppermost curve corresponds to the low-localization zone, between the ϵ_0 and the ϵ_b light lines.

The typical behaviors of the fields corresponding to the surface modes in a superlattice are displayed in Fig. 6. The electric-field profiles $E(x, 0)$ are obtained by Eqs. (4) and (6) for TE waves. We clearly observe that the energy is localized at the uppermost cells, two or three cells away from the interface. On the side of the air the confinement is stronger. In fact, the decay distance of the fields in the air is $\sim d$. This is an important point because it is one of the requirements of the supercell method that this decay distance be substantially smaller than l_0. Here we used $l_0 = 0.25l$ for the width of the air layers. This separation is sufficient to guarantee that there be no appreciable overlap of the fields in two neighboring supercell slabs. It is necessary to say that the thickness of the air regions does not represent a problem for the convergence of the numerical solutions. In fact, for $l_0 > 2d$ the solutions become independent of l_0.

We can also appreciate in Fig. 6 the different oscillation patterns of the fields corresponding to surface modes located in different band gaps. Of course the bulk bands of Figs. 5(a) and 5(b) result from the coupling of the modes of all the guiding layers of dielectric constant ϵ_a. The coupling of the lowest (even) modes of these layers gives

rise to the first bulk band; the coupling of the second modes of all the layers (odd modes) gives rise to the second bulk band, and so on. When the superlattice is terminated with the surface at $\tau = 0.75$, the modes corresponding to the last (incomplete) ϵ_a layer differ in frequency and field amplitude from those of the ϵ_a layers of the interior of the superlattice. Therefore the surface-cell modes cannot be coupled with the inner-cell modes of any bulk band, giving rise to isolated states (the surface modes). On the other hand, the oscillations of the fields in the last ϵ_a layer are similar to the field patterns of the modes in a single dielectric slab, although modified by the presence of the semi-infinite superlattice. Thus in the last ϵ_a layer the profile of the field amplitude of the lowest-frequency surface wave is similar to an even function without nodes. The second surface mode resembles an odd function with one node, and so on. The propagation wave-vector continuity produces a similar oscillation pattern for the field intensity in all the inner ϵ_a layers. Their amplitude, however, decreases from layer to layer in the direction of penetration.

The localization of a surface mode depends on the position of its dispersion relation in the plane β–ω. Within the same dispersion branch the surface modes can run from a zone of low localization at the surface (dispersion relation lying between the air light line and the ϵ_b light line) to a zone of high localization (dispersion relation lying to the right side of the ϵ_b light line), as we can see in Figs. 5(a) and 5(b). In both zones the closeness between the dispersion relation and the band edges is another factor that affects the penetration of the fields into the superlattice. We plot in Fig. 7 two electric-field profiles corresponding to different points of the third dispersion curve of Fig. 5(a). One lies in the low-localization zone and the other in the high-localization zone. The figure clearly shows the different confinements of the waves (in both the air and the superlattice sides). This difference

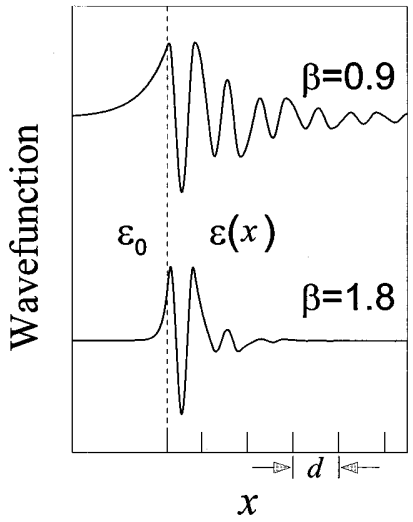

Fig. 7. Electric-field profiles of two surface modes for the third dispersion curve of Fig. 5(a). The dashed line is the superlattice–air interface. The figure shows the variation of the field confinement of modes lying in the low-localization zone ($\beta = 0.9$) and the high-localization zone ($\beta = 1.8$).

Table 1. Attenuation Coefficient α and Penetration Depth δ of Three Modes (β, ω) on the Third Dispersion Curve of Fig. 5(a)

β	ω	αd	δ/d
0.90	0.853	0.685	1.459
1.30	0.981	1.079	0.926
1.70	1.117	1.740	0.574

is because, in the zone of low localization, the modes are in the vicinity of the air light line and the fields oscillate in both media ϵ_a and ϵ_b (in the direction perpendicular to the surface). On the other hand, in the zone of high localization the fields oscillate only in the medium ϵ_a and they are distant from the air light line.

In order to quantify these considerations, we evaluated the attenuation coefficient α and the penetration depth (into the superlattice) $\delta = 1/\alpha$ for the surface waves. In general, the extremum value of the field amplitude of the surface modes does not coincide with the air–superlattice interface. We assumed an $\exp(-x/\delta)$ dependence of the envelope and measured δ from the position of the extreme value in the surface cell. Thus the attenuation coefficient is related to the exponential damping of the local extreme value of the field intensity in every cell. The α value, obtained by this procedure, must approach the imaginary part of the respective Bloch wave vector in the semi-infinite superlattice. We show in Table 1 results obtained for three points on the third dispersion curve of Fig. 5(a). Running from the low-localization zone to the high-localization zone, the attenuation coefficient (the penetration depth) increases (decreases) rapidly. From the data given in Table 1 we note that for $\beta = 0.9$ the penetration is almost 2.5 times greater than for $\beta = 1.7$.

As we mentioned previously, the penetration depth in the superlattice depends as much on the closeness between the band edges and the dispersion curve as on the zone, of high or low localization, where this dispersion curve is located. A mode very near to a band edge is very penetrating. On the other hand, the confinement of the fields is maximum for frequencies at the center of a band gap. We observed, for example, for the first dispersion curve in Fig. 5(a), a very long penetration depth at $\beta = 0.9$ (located almost at the upper band edge), which contrasts with the localization obtained for $\beta = 1.2$ (see the lowest profile in Fig. 6). This behavior is related to the imaginary part of the Bloch wave vector in the superlattice that varies from zero at the band edges to a maximum at the center of the band gap.

We will see in Subsection 3.C that the positions of the surface dispersion curves in all the band gaps depend on the cut parameter value τ. In Fig. 5(a) the first surface mode is located near a band edge, and the third surface mode is located at the center of the gap. With a slight change of τ the first mode can move to frequency regions of higher or lower confinement, whereas the third mode can move only to regions of higher penetration.

C. Dependence of the Surface Modes on the Termination of the Superlattice

Next we investigate how the position of the surface (i.e., the structure of the surface cell in the superlattice) affects

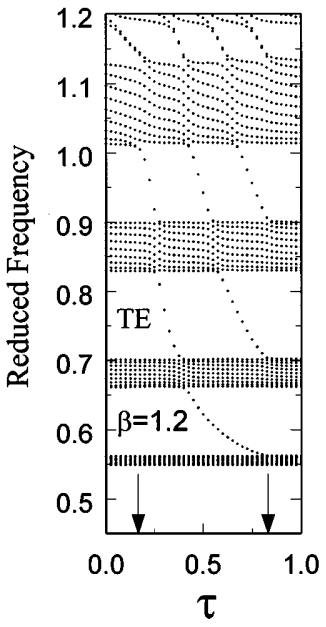

Fig. 8. TE surface-modes behavior as a function of the cut distance in the surface cell (TiO_2/SiO_2 superlattice). The interval $0 \leqslant \tau \leqslant 1$ corresponds to the unit cell width. The two arrows at the bottom of the figure (which delimit three regions in the cell) are the limits of the layer of dielectric constant ϵ_a. By increasing τ, modes are lowered from the bulk bands and become surface modes. There are no surface modes for $\tau > b/2d + a/d = 0.833$.

the surface-mode eigenfrequencies. For TE polarization, in Fig. 8 we show ω as a function of the cut parameter τ for a fixed β (= 1.2). The two arrows in the figure delimit the width of the layer with dielectric constant ϵ_a of the unit cell. When the τ value is selected, a surface cell of width τd is defined. For example, for $\tau = 0.5$ the surface cell is constituted by an ϵ_b layer of thickness $b/2$ and an ϵ_a layer of thickness $a/2$ (the ϵ_a layer at the surface has one-half the bulk width). For any band gap we observe that surface modes do not occur for all the range of τ values. In fact, in the lower three band gaps they appear only when the truncation of the superlattice is realized through the ϵ_a layer. This, however, is not a sufficient condition for the existence of surface waves.

When the superlattice terminates with a complete unitary cell (in Fig. 8, $\tau = 0$ or $\tau = 1$), there are no solutions within the band gaps. Hence in this case the parameters used do not give rise to surface waves. However, by increasing τ a little, such solutions begin to appear. Below, we analyze the results for TE modes in the three regions of τd already considered in Eq. (12) and Fig. 3.

Region (a). $0 < \tau d \leqslant b/2$ ($0 < \tau < 0.166$); Fig. 3(a). We observe in Fig. 8 that a TE electromagnetic mode is peeled off from the bottom of the fifth band. The mode becomes a surface mode and sweeps almost the complete fourth band gap. No other surface mode appears in any other band gap.

These surface solutions lie in the low-localization zone [see the bulk-band structure of Fig. 5(a) for $\beta = 1.2$]. The profile of the mode with $\tau = 0.12$ displayed in Fig. 9 reveals considerable penetration into the superlattice. We note that the field is maximal at the surface layer of dielectric constant ϵ_b.

Region (b). $b/2 < \tau d \leqslant b/2 + a$ ($0.166 < \tau \leqslant 0.833$); Fig. 3(b). The surface modes exist in every band gap. They can be considered as the guided eigenmodes of the surface ϵ_a layer, modified by the presence of the semi-infinite superlattice. When the thickness of this layer is increased from zero to a (varying τd from $b/2$ to $b/2 + a$), the frequencies of these modes are lowered. Thus the modes associated with the surface cell undergo a falling process from higher frequencies until they merge with an appropriated bulk band. We note in Fig. 8 that at the same τ value at which a surface mode of the fourth band gap disappears, $\tau \sim b/2d$, one mode is lowered from the bottom of the fourth bulk band (frequency ~1.01), becoming a surface mode. As τ is increased, this mode sweeps through the third, the second, and the first band gaps until it reaches the lower bulk band and disappears, acquiring the propagatory character of the bulk solutions of the first band. As the thickness of the ϵ_a layer is increased, we also see three other modes lowered from the fifth bulk band and becoming surface modes. These three modes come to merge with different bands (the second, the third, and the fourth bulk bands, respectively). Thus we can clearly appreciate that, for an almost complete ϵ_a layer, one bulk mode is added to each band as a result of increasing the termination of the superlattice.

Region (c). $b/2 + a < \tau d \leqslant d$ ($0.833 < \tau \leqslant 1$); Fig. 3(c). There are no surface modes for the parameters considered.

The behavior of the TE surface modes that we described in the three regions of Fig. 8 is not general. Thus for TM waves with $\beta = 0.9$ a surface mode clearly persists for $\tau d \geqslant b/2 + a$ (see Fig. 10). This means that for suitable parameters and polarization the surface modes can also exist in region (c). As an additional example, in Fig. 11 we present the field profiles of two surface waves

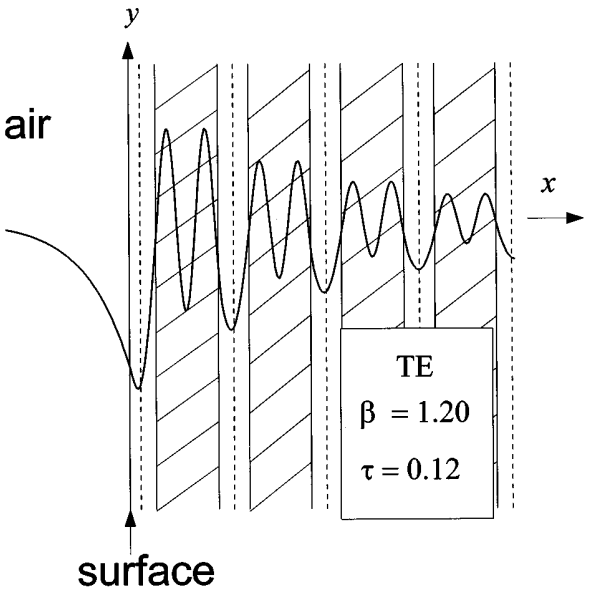

Fig. 9. Electric-field profile Re(E) of a surface wave with the greatest extremum in the surface ϵ_b layer.

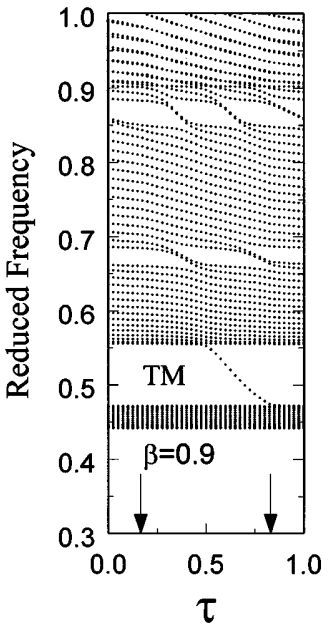

Fig. 10. As in Fig. 8 but for TM polarization, $\beta = 0.9$, and $n = 15$.

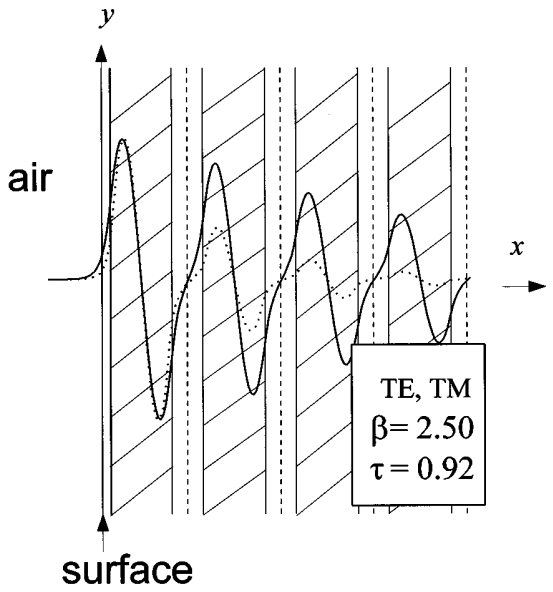

Fig. 11. Electric-field profile Re(E) (continuous curve) and magnetic-field profile Re(H) (dotted curve) of surface waves with their local maximum in the second layer from the surface (the first ϵ_a layer).

in region (c) for a very large propagation vector ($\tau = 0.92$ and $\beta = 2.5$). These TE and TM modes, which appear in the second band gap and are represented by continuous and dashed curves, respectively, are weakly localized oscillations of essentially odd character within every guiding layer ϵ_a. Their largest field maxima are located in the second layer from the surface (the first ϵ_a layer).

In order to generalize the conditions for the existence of surface modes in a TiO_2/SiO_2 superlattice, in Figs. 12 and 13 we show the τ regions in which such modes appear in the lower three band gaps. The figures correspond to $\beta = 0.9$ and $\beta = 1.5$, respectively. For both TE and TM waves, we shaded the τ intervals at which the separation of the surface mode from the bulk bands is well defined. For any shaded region, the left (right) boundary corresponds to a frequency just below (above) the upper (lower) bulk band delimiting the respective band gap (see Figs. 8 and 10). We remind the reader that a surface layer with dielectric constant ϵ_a lies in the region (b), $0.166 \leqslant \tau \leqslant 0.833$. When the cutoff position is outside this interval (i.e., the truncation of the superlattice is realized through the ϵ_b layer), for $\beta = 0.9$ the surface modes appear for both TE and TM waves only in the third band gap (the highest gap below the light line for this propagation vector). For $\beta = 1.5$ they appear outside region (b) only for TM polarization in the very narrow range $0.833 < \tau < 0.85$ in all the three band gaps. With $\beta > 1.5$ we observed similar behavior for both polarizations as in Fig. 13, but propagation of TM waves in the third region ($\tau > 0.833$) is possible for greater values of τ. On the other hand, it can be appreciated that a TM solution in the third band gap in Fig. 12 exists even in the limit of a complete surface cell ($\tau = 0$ or $\tau = 1$). In fact, it is the only

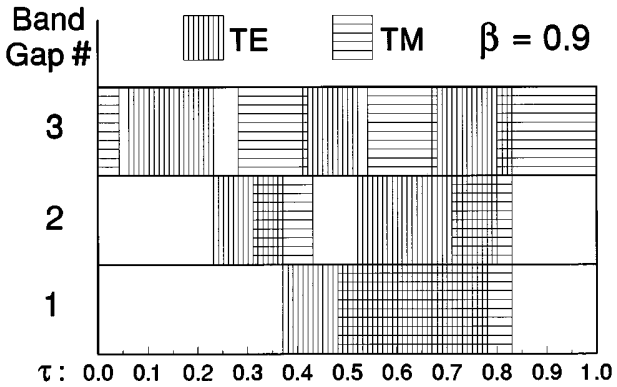

Fig. 12. Representation of the τ regions in which surface modes appear for $\beta = 0.9$ in the lower three band gaps of the band structure in Figs. 5(a) and 5(b).

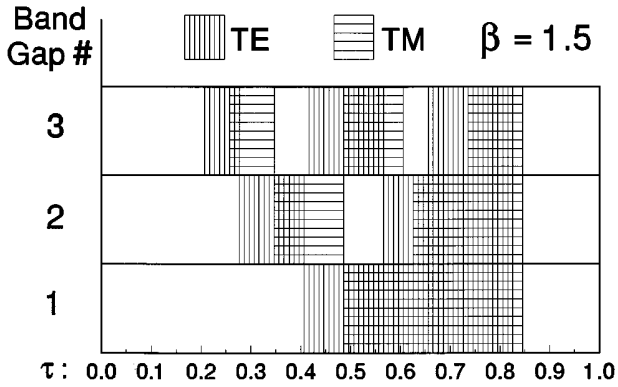

Fig. 13. Same as Fig. 12 but for $\beta = 1.5$.

mode appearing in this limit. Because the surface unit cell is complete, these modes exist only because of the termination of the superlattice (in the language of solid-state physics, surface reconstruction is disregarded). All the other surface solutions discussed in this paper are associated with surface reconstruction ($\tau \neq 0$ or, equivalently, $\tau \neq 1$).

The TM modes just mentioned appeared in all the band gaps (for different β ranges), and the band crossing points give the upper limit for β (see Fig. 14 for $\tau = 1$ and $n = 13$). This behavior is related to the internal (between the layers) Brewster effect. In Fig. 14, for the solution in the first band gap, we plot the two curves of dispersion corresponding to the modes at the two surfaces of the superlattice slab. Apparently in this case, $n = 13$ is not sufficiently large to eliminate the interaction of these two modes. We observed that the separation closes by increasing n. Also, no surface modes appear to the right of a crossing point. This and other types of propagation constant-limited modes will be the topic of future study.

Finally, we studied the surface waves in a superlattice of low dielectric contrast between the layers (parameters discussed at the beginning of Section 3). We found that the behavior is not very different from that shown in Figs. 12 and 13. On the other hand, we presented results for a TiO_2/SiO_2 superlattice only for $b = 0.5a$ (i.e., filling fraction $f = a/d = 0.66$). If we change this b value, both the bulk- and the surface-band structures will be modified. Larger (smaller) b leads to narrow (wide) bulk bands. In any case, surface modes must appear for some terminations of the superlattice. We do not expect a behavior qualitatively different than that discussed in this paper.

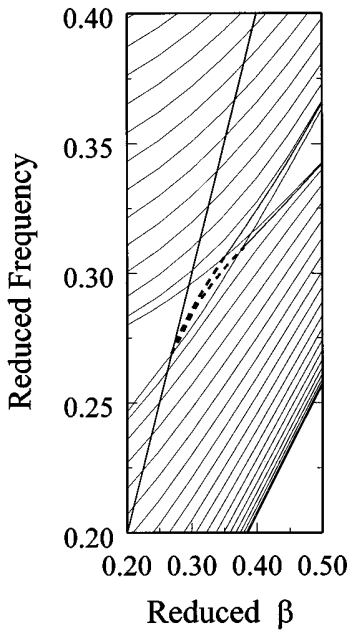

Fig. 14. Detail of Fig. 5(b) showing parts of the two lower bands. Surface modes (dashed curves) appear in the band gap assuming that the cell next to the surface is a complete bulk cell ($\tau = 1$). The graph is obtained with a slab of $n = 13$ complete cells. For $n \to \infty$ the two dashed curves coalesce and terminate at the intersection point of the bulk bands.

4. SUMMARY AND CONCLUSION

We have presented in detail the supercell method as applied to the calculation of electromagnetic surface modes of a dielectric superlattice. By the construction of a supercell containing a (finite) slab of superlattice, we demonstrated numerically that this method leads to the same dispersion relations as those obtained by another theory, for the semi-infinite problem. We studied the conditions for agreement as a function of the number of cells n in the slab and the lattice constant. With the exception of one special type of TM surface modes, good accuracy is reached already with $n = 7$.

Particular superlattices studied were GaAs/AlGaAs and TiO_2/SiO_2 of dielectric constants 11.42/8.35 and 5.52/2.13, respectively. Our results can be summarized as follows. The surface waves, for both TE and TM polarizations, are strongly dependent on the superlattice termination. By introducing the cut parameter τ ($0 \leqslant \tau \leqslant 1$), we have computed these waves as a function of the position of the surface (parallel to the layer interfaces) in the centrosymmetric unit cell of width $d = a + b$. The surface can cut the superlattice through the ϵ_b medium ($0 \leqslant \tau d \leqslant b/2$ and $a + b/2 \leqslant \tau d \leqslant d$) or through the ϵ_a medium ($b/2 < \tau d < a + b/2$). For fixed propagation vector β we studied the behavior of the surface modes as τ is varied. In every band gap, only one mode exists. For small τ we found a surface solution in the highest relevant band gap (the first band gap below the light line). The maximum of the field profile of this mode lies in the surface layer of dielectric constant ϵ_b. As τ is increased, the frequency of this mode is lowered, reaching the inferior band gaps. At the same time its field profile undergoes modifications, and other surface modes appear. Their frequencies are also lowered with increasing τ. For $\tau d \sim a + b/2$, one mode occurs in every band gap. They all lie just above a bulk band, with the field extremum in the surface layer of dielectric constant ϵ_a. For modes with τ slightly larger than this value, a superlattice with a very thin ϵ_b layer at the surface, the maximum of the field profile also lies in the first ϵ_a layer (the second layer away the surface). The TM surface modes appearing to the left side of the Brewster light line are the only modes that exist in the absence of surface reconstruction (that is, for a complete unit cell at the surface). These are very penetrating modes.

In conclusion, the results presented in this paper validate the applicability of the supercell method for electromagnetic surface-mode calculations. The dependence of these waves, their dispersion relation and field amplitude, on the superlattice termination can be studied with the numerical precision desired.

ACKNOWLEDGMENTS

We thank J. A. Gaspar for his generous help in the computation at the beginning of this work and for general discussions. F. Ramos-Mendieta wishes to thank the Universidad Autónoma de Puebla for hospitality. This project is supported by Consejo Nacional de Ciencia y Tecnología grant 3923-E9402.

REFERENCES

1. R. E. Camley, B. Djafari-Rouhani, L. Dobrzynski, and A. A. Maradudin, "Transverse elastic waves in periodically layered infinite and semi-infinite media," Phys. Rev. B **27**, 7318 (1983).
2. R. E. Camley and D. L. Mills, "Collective excitations of semi-infinite superlattice structure: surface plasmon, bulk plasmons, and the electron-energy-loss spectrum," Phys. Rev. B **29**, 1695 (1984).
3. E. L. Albuquerque and M. G. Cottam, "Superlattice plasmon-polaritons," Phys. Rep. **233**(2), 67 (1993).
4. L. H. Qin, Y. D. Zheng, and R. Zhang, "Study of Ge_xSi_{1-x}/Si superlattices by ellipsometry," Appl. Phys. A **55**, 297 (1992).
5. T. Hattori, N. Tsurumachi, S. Kawato, and H. Nakatsuka, "Photonic dispersion relation in a one-dimensional quasicrystal," Phys. Rev. B **50**, 4220 (1994).
6. P. Yeh, A. Yariv, and C.-S. Hong, "Electromagnetic propagation in periodic stratified media. I. General theory," J. Opt. Soc. Am. **67**, 423 (1977).
7. A. Yariv and P. Yeh, *Optical Waves in Crystals* (Wiley, New York, 1984).
8. M. L. Bah, A. Akjouj, and L. Dobrzynski, "Response functions in layered dielectric media," Surf. Sci. Rep. **16**, 95 (1992).
9. J. P. Dowling and C. M. Bowden, "Atomic emission rates in inhomogeneous media with applications to photonic band structures," Phys. Rev. A **46**, 612 (1992).
10. J. P. Dowling and C. M. Bowden, "Beat radiation from dipoles near a photonic band edge," J. Opt. Soc. Am. B **10**, 353 (1993).
11. R. D. Meade, K. D. Brommer, A. M. Rappe, and J. D. Joannopoulos, "Electromagnetic Bloch waves at the surface of a photonic crystal," Phys. Rev. B **44**, 10961 (1991).
12. D. Kossel, "Analogies between thin-film optics and electron-band theory of solids," J. Opt. Soc. Am. **56**, 1434 (1966).
13. P. Yeh, A. Yariv, and A. Y. Cho, "Optical surface waves in periodic layered media," Appl. Phys. Lett. **32**, 104 (1978).
14. W. Ng, P. Yeh, P. C. Chen, and A. Yariv, "Optical surface waves in periodic layered medium grown by liquid phase epitaxy," Appl. Phys. Lett. **32**, 370 (1978).
15. A. A. Bulgakov and V. R. Kovtun, "Surface optical oscillations in a bounded layered-periodic medium," Opt. Spektrosk. **56**, 769 (1984).
16. R. Haupt and L. Wendler, "Dispersion and damping properties of plasmon polaritons in superlattice structures," Phys. Status Solidi B **142**, 423 (1987); M. S. Kushwaha, "Intrasubband plasmons in semi-infinite n-i-p-i semiconductor superlattice," Phys. Rev. B **45**, 6050 (1992); R. F. Wallis, R. Szenics, J. J. Quinn, and G. F. Giuliani, "Theory of surface magnetoplasmon polaritons in truncated superlattices," Phys. Rev. B **36**, 1218 (1987).
17. W. L. Bloss, "Surface states of a semi-infinite superlattice," Phys. Rev. B **44**, 8035 (1990).
18. X. I. Saldaña and G. González de la Cruz, "Electromagnetic surface waves in semi-infinite superlattices," J. Opt. Soc. Am. A **8**, 36 (1991).
19. P. Yeh, *Optical Waves in Layered Media* (Wiley, New York, 1988).
20. A. V. Vinogradov and I. V. Kozhevnikov, "X-ray surface waves in a superlattice," JETP Lett. **40**, 1222 (1984).
21. R. F. Wallis, "Surface phonons: theoretical developments," Surf. Sci. **299/300**, 612 (1994).
22. W. M. Robertson, G. Arjavalingam, R. D. Meade, K. D. Brommer, A. M. Rappe, and J. D. Joannopoulos, "Observation of surface photons on periodic dielectric arrays," Opt. Lett. **18**, 528 (1993).